HHS Public Access

Author manuscript

Small. Author manuscript; available in PMC 2019 January 01.

Published in final edited form as:

Small. 2018 January ; 14(3): . doi:10.1002/smll.201701828.

Detection of β-Amyloid by Sialic Acid Coated Bovine Serum Albumin Magnetic Nanoparticles in a Mouse Model of Alzheimer's Disease

Seyedmehdi Hossaini Nasr,
Department of Chemistry, Michigan State University, 578 S. Shaw Lane, East Lansing, MI 48824, USA

Dr. Hovig Kouyoumdjian,
Department of Chemistry, Michigan State University, 578 S. Shaw Lane, East Lansing, MI 48824, USA. Department of Chemistry, York University, 4700 Keele Street, Chemistry Building 350, Toronto, ON M3J 1P3 T, Canada

Dr. Christiane Mallett,
Department of Radiology, Michigan State University, East Lansing, MI 48824, USA

Dr. Sherif Ramadan,
Department of Chemistry, Michigan State University, 578 S. Shaw Lane, East Lansing, MI 48824, USA. Chemistry Department, Faculty of Science, Benha University, Benha, Qaliobiya 13518, Egypt

Prof. David C. Zhu,
Department of Radiology, Michigan State University, East Lansing, MI 48824, USA

Prof. Erik M. Shapiro, and
Department of Radiology, Michigan State University, East Lansing, MI 48824, USA. Department of Biomedical Engineering and Institute for Quantitative, Health Science and Engineering, Michigan State University, East Lansing, MI 48824, USA

Prof. Xuefei Huang
Department of Chemistry, Michigan State University, 578 S. Shaw Lane, East Lansing, MI 48824, USA. Department of Biomedical Engineering and Institute for Quantitative, Health Science and Engineering, Michigan State University, East Lansing, MI 48824, USA

Abstract

The accumulation and formation of β-amyloid (Aβ) plaques in the brain are distinctive pathological hallmarks of Alzheimer's disease (AD). Designing nanoparticle (NP) contrast agents capable of binding with Aβ highly selectively can potentially facilitate early detection of AD.

Correspondence to: Xuefei Huang.

The ORCID identification number(s) for the author(s) of this article can be found under https://doi.org/10.1002/smll.201701828.

Conflict of Interest
The authors declare no conflict of interest.

Supporting Information
Supporting Information is available from the Wiley Online Library or from the author.

However, a significant obstacle is the blood brain barrier (BBB), which can preclude the entrance of NPs into the brain for Aβ binding. In this work, bovine serum albumin (BSA) coated NPs are decorated with sialic acid (NP-BSA$_x$-Sia) to overcome the challenges in Aβ imaging in vivo. The NP-BSA$_x$-Sia is biocompatible with high magnetic relaxivities, suggesting that they are suitable contrast agents for magnetic resonance imaging (MRI). The NP-BSA$_x$-Sia binds with Aβ in a sialic acid dependent manner with high selectivities toward Aβ deposited on brains and cross the BBB in an in vitro model. The abilities of these NPs to detect Aβ in vivo in human AD transgenic mice by MRI are evaluated without the need to coinject mannitol to increase BBB permeability. T_2*-weighted MRI shows that Aβ plaques in mouse brains can be detected as aided by NPBSA$_x$-Sia, which is confirmed by histological analysis. Thus, NP-BSA$_x$-Sia is a promising new tool for noninvasive in vivo detection of Aβ plaques.

Keywords

β-amyloid; blood brain barrier; magnetic nanoparticles; magnetic resonance imaging; sialic acid

1. Introduction

Alzheimer's disease (AD) is the most common type of dementia. Studies by the Alzheimer's Disease International Institute indicate that in 2016, about 47 million people worldwide lived with dementia and this number is expected to rise to 132 million in 2050.[1,2] The economic impact of AD is estimated to be $818 billion in 2016. These staggering numbers suggest that new methods for diagnosis and treatment of AD are urgently needed, and early detection of AD can potentially improve the prognosis for AD patients.[3,4]

The accumulation and deposition of β-amyloid (Aβ) peptides in brain tissues are one of the most distinctive hallmarks of AD.[5] Strong correlations have been found between Aβ deposition and the beginning of atrophy at early stage of AD.[6] As a result, Aβ has been an attractive target for the development of noninvasive methods for AD detection. Positron emission tomography (PET) has been used clinically for AD brain imaging.[7] Pittsburgh compound-B[8,9] is a ^{11}C containing PET tracer that can selectively bind with β-sheeted Aβ aggregates, which has been approved by the Food and Drug Administration (FDA) for imaging Aβ plaques in brains. However, PET has inherent low spatial resolution and utilizes ionizing radiation. An appealing alternative for Aβ imaging is magnetic resonance imaging (MRI) due to its noninvasive nature and high spatial resolution. Advanced Aβ plaques can be detected directly via MRI due to the accumulation of iron ions in plaque tissues, leading to contrast changes from the surrounding tissues.[10–13] For early plaque detection, the inherent contrast associated with the plaques is not sufficient. Thus, contrast agents are needed to enable plaque imaging by MRI, which are most commonly delivered by nanoparticles (NPs).[14–19]

One significant challenge in Aβ imaging using NP contrast agents is the blood brain barrier (BBB), which has tight junctions between endothelial cells lining the blood vessels in the brain[20,21] and severely limits entries of macromolecules such as NPs into brains.[20,22] In order to overcome this, a common approach is to add mannitol into the NP formulation,

which transiently opens up the BBB, allowing particles to diffuse into brain tissues.[23,24] However, it is challenging to apply this approach to humans due to the concern for possible brain infections with the opened BBB. NPs that are able to penetrate the BBB without the need for mannitol are desirable for Aβ imaging.

To facilitate selective binding of NPs to Aβ plaques, Aβ targeting agents are needed to functionalize the NPs. The most extensively utilized ones are either full length or fragments Aβ as these peptides can aggregate with Aβ plaques, thus enriching contrast agents in plaque sites.[14,17,18,24,25] Wadghiri et al. pioneered Aβ coated magnetic NPs to image Aβ in mouse models of AD.[17] A potential drawback using Aβ-based targeting vectors is the concern that they can possibly lead to further growth of plaques. Alternatively, Aβ binding monoclonal antibodies (mAbs) have been explored as targeting agents.[26] However, besides their high costs and potential immunogenicities, the use of mAbs has side effects.[27] For instance, the administration of anti-Aβ mAbs Bapineuzumab and Gantenerumab increased the risk of amyloid related imaging abnormalities of brains, including chronic brain hemorrhages and swelling of brains.[28,29] Small molecules such as curcumin[30] and Congo red[31] have been tested as Aβ targeting agents. NPs bearing these ligands require mannitol to facilitate their entries into brain tissues.

Sialic acid is an interesting ligand for Aβ binding studies.[32] Sialic acid is a monosaccharide with a nine-carbon backbone, which is mostly found at terminal ends of saccharide chains such as gangliosides rich in the nervous system.[33] Located on neuronal membranes, monosialotetrahexosyl ganglioside (GM1) is the most abundant ganglioside in the brain. Studies have shown that residues His13 to Leu17 located at the *N*-terminal of the Aβ peptide are important for their interactions with GM1 and His13 is responsible for specific interaction with the sialic acid moiety of GM1.[34–37] By binding with Aβ, exogenous GM1 can inhibit Aβ induced cytokine release and inflammatory responses by neuronal cells.[38] The intrinsic ability of sialic acid to bind with Aβ fibrils and its biocompatibility make it suitable for Aβ studies, especially when multiple copies of it can be placed on a nanostructure, resulting in enhanced avidities.[32] Sialic acid conjugated second generation polyamidoamine (PAMAM) dendrimers were found to decrease Aβ toxicity toward SH-SY5Y neuroblastoma cells.[39,40] While increasing the multivalency of these dendrimers improved Aβ binding, third and fourth generation PAMAM dendrimers caused cell death due to their inherent cellular toxicities, limiting their utility in vivo. Other sialic acid bearing NP platforms investigated for Aβ studies include gold nanoshells deposited on carbon electrode,[41] chitosan polysaccharides,[42] and magnetic NPs.[43] No in vivo studies have been reported using these constructs presumably due to either the inherent toxicity of the carrier or the limited abilities to pass the BBB.[39,42,44]

Herein, we report the synthesis of sialic-acid-functionalized bovine serum albumin (BSA) coated magnetic NPs (NP-BSA$_x$-Sia). As crossing BBB is a significant barrier for brain imaging, NP-BSA$_x$-Sia can overcome this roadblock, pass through BBB, and bind with Aβ peptide with high selectivities. Furthermore, administration of this probe to AD mice enables in vivo detection of AD plaques through MRI without the need for mannitol to open the BBB. This is the first time that sialic acid NPs have been utilized to image Aβ in vivo. The high biocompatibility, magnetic relaxivity, and Aβ selectivity coupled with its ability to

cross the BBB render NP-BSA$_x$-Sia a promising contrast agent for noninvasive imaging of Aβ.

2. Results

2.1. Synthesis and Characterization of NP-BSA$_x$-Sia

The synthesis of NP-BSA$_x$-Sia started from the preparation of iron oxide NPs through the thermal decomposition method.[45] Heating a mixture of Fe(acac)$_2$ and hexadecanediol in the presence of oleic acid and oleylamine from 200 to 300 °C in benzyl ether formed magnetite NPs (Figure 1). The hydrophobic particles were rendered water soluble through ligand exchange with tetramethylammonium hydroxide (TMAOH) followed by incubation with BSA,[46] which can noncovalently absorb on the surface of the NPs providing a protein layer for further functionalization. The resulting NPs were incubated with 2,2′-(ethylenedioxy)bis(ethylamine) **1** and ethyl-(3,3-dimethylaminopropyl) carbodiimide hydrochloride (EDCI), which could covalently crosslink the carboxylic acids of immobilized BSA through amide bond formation, leading to NP-BSA$_x$. Sialic acid was then introduced onto the NPs through EDCI mediated amide bond formation with sialic acid derivative **2,**[43] followed by subsequent ester hydrolysis generating the NP-BSA$_x$-Sia. The prepared NPs were further labeled when needed with the fluorophore fluorescein isothiocyanate (FITC) by presumably reacting with residual amines on NP-BSA$_x$-Sia to form NP-BSA$_x$-Sia-FITC, enabling their tracking by fluorescence for cellular experiments.

The NPs were characterized with a variety of methods. The average core diameters of the NPs were 5 nm as determined by transmission electron microscopy (TEM) (Figure 1) with an average hydrodynamic diameter of 87 nm in phosphate buffered saline (PBS) buffer analyzed by dynamic light scattering. The cationization of BSA through amination is important to facilitate BBB crossing.[46,47] Zeta potential (ζ) surface charge measurements was a convenient method to monitor the amination process. The BSA coated magnetic NPs as synthesized had a negative zeta potential of −6.6 mV in PBS buffer. Upon reaction with diamine **1**, ζ values increased to +11.2 mV, suggesting the successful introduction of amines onto the NPs. The number of 2,2′-(ethylenedioxy)bis(ethylamine) that reacted with BSA was analyzed by mass spectrometry of BSA functionalized in solution under the identical reaction condition as NP modification. Based on the molecular weight difference of BSA before and after functionalization, the average number of diamine **1** introduced was estimated to be 33 per BSA molecule (Figure S1a, Supporting Information). Amidation of NP-BSA$_x$ with sialic acid lowered the ζ value to +5.2 mV, indicating the conversion of some of the positively charged amines to neutral amides. The total organic content was determined by thermogravimetric analysis to be 74% of the weight of the NP-BSA$_x$-Sia (Figure S1b, Supporting Information). The amount of sialic acid on NP-BSA$_x$-Sia was quantified by thiobarbituric acid assay[48] following mild acid treatment of the NPs to cleave off the sialic acid. The amount of sialic acid accounted for 7% of the weight of NPs with an average of 118 sialic acid molecules per NP-BSA$_x$-Sia. The NP-BSA$_x$-Sia has high magnetic relaxivities with an r_2* value of 220 L mmol^{-1} s^{-1} (7 Tesla), suggesting that these particles are good T_2*-based MRI contrast agents (Figure S1c, Supporting Information). The NPs are

colloidally stable as there were little changes in their hydrodynamic sizes or surface charges when kept in solution for more than three weeks (Figure S1d, Supporting Information).

2.2. NP-BSA$_x$-Sia was Biocompatible and Nontoxic to Cells

For in vivo applications of NPs, it is critical that the particles are biocompatible. Brain endothelial cells are a critical component of the BBB that controls passages of exogenous molecules into the brain.[49] Damages to this barrier can expose the brain to a variety of harmful compounds that are normally excluded from the brain. To evaluate their biocompatibilities, NP-BSA$_x$-Sia and NP-BSA$_x$ were incubated with brain endothelial cells bEnd.3 and their effects on cell viabilities were analyzed using the 3-(4,5-dimethylthiazol-2-yl)-5-(3-carboxy-methoxyphenyl)-2-(4-sulfophenyl)-2H-tetrazolium cell viability assay. As shown in Figure 2, with concentrations examined up to 1 mg mL^{-1}, NP-BSA$_x$-Sia did not have any adverse effects on cell viability. In contrast, cells incubated with NP-BSA$_x$ above 0.25 mg mL^{-1} exhibited reduced viability with only 40% alive at 1 mg mL^{-1} of NP-BSA$_x$. These results indicate that NP-BSA$_x$-Sia has good biocompatibility and NP-BSA$_x$ is not suitable for in vivo applications due to potential toxicities.

2.3. NP-BSA$_x$-Sia was Taken Up by bEnd.3 Brain Endothelial Cells and Internalized NPs could be Released from the Cells

The interactions of NP-BSA$_x$-Sia with brain endothelial cells bEnd.3 were analyzed next using FITC labeled NP-BSA$_x$-Sia NPs for fluorescence monitoring. Upon incubation with bEnd.3 cells for 1, 3, and 7 h followed by thorough washes to remove unbound NPs, flow cytometry analysis of the cells was performed (Figure 3a). Even with 1 h incubation, there was significant fluorescence associated with the cells. Larger increases of cellular fluorescence intensities were observed after 3 and 7 h of incubation. The cells were then imaged with confocal microscopy after FITC-NP incubation, which showed extensive green fluorescence in the cytoplasm of the cells (Figure 3b–g), suggesting that NP-BSA$_x$-Sia was internalized by brain endothelial cells bEnd.3.

After uptake, the fate of intracellular NPs was studied. Cells loaded with the NP-BSA$_x$-Sia-FITC were washed to remove any free or surface bound NPs and incubated in fresh media without any exogenous NPs. The extracellular fluorescence was continuously monitored, which showed a time dependent increase with a half-life of 5 h (Figure 4a). These results indicate that NP-BSA$_x$-Sia taken up by bEnd.3 cells can be released from the cells.

2.4. NP-BSA$_x$-Sia was able to Cross BBB In Vitro as Established in a Transwell Assay

Having demonstrated that NP-BSA$_x$-Sia can be taken up and subsequently released by bEnd.3 cells, we envision that combining these processes can potentially facilitate BBB crossing by the NPs. An in vitro BBB model was established by growing multiple layers of brain vascular endothelial bEnd.3 cells on the filter of a transwell. Transendothelial electrical resistance (TEER) measurements showed an average electrical resistance value of 133 Ω cm^{-2} across the multicellular layers (Figure S2a, Supporting Information), indicating that tight junctions were formed between the cells mimicking BBB.[50,51] NP-BSA$_x$-Sia-FITC (0.32 mg mL^{-1}) was added to one side of the chamber and the fluorescence across the multilayer of cells was continuously monitored. As shown in Figure 4b, significant increase of

fluorescence intensity was observed, indicating that the NPs can be transported through multilayers of brain endothelial cells. The NPs did not affect much the tight junctions between the cells as there were little changes in the electrical resistance across the cell layers through this experiment (Figure S2b, Supporting Information).

2.5. NP-BSA$_x$-Sia could Bind with Aβ in a Sialic Acid Dependent Manner

Aβ (1-42) is a major component of amyloid peptides in the senile plaques in AD brains and it is considered the most toxic Aβ forms.[52] Due to its importance in AD, its interaction with NP-BSA$_x$-Sia was studied. NP-BSA$_x$-Sia was immobilized on a microtiter plate and increasing concentrations of Aβ fibrils were added to wells containing NP-BSA$_x$-Sia. After removal of unbound Aβ, dose dependent increase of absorbance was observed upon addition of an anti-Aβ mAb followed by horseradish peroxide (HRP) conjugated secondary antibody (Figure 5a). The apparent dissociation constant between Aβ and NP-BSA$_x$-Sia was 3×10^{-6} M. In comparison, very little Aβ was found in wells not containing NP-BSA$_x$-Sia. Besides Aβ fibrils, Aβ can also exist in oligomeric forms, which may be an important contributor to neurotoxicity.[53–59] NP-BSA$_x$-Sia can also bind with Aβ oligomers as illustrated by enzyme-linked immunosorbent assay (ELISA) (Figure S3, Supporting Information).

To understand the role of sialic acid in Aβ binding, a competitive ELISA was performed. After introducing a constant amount of Aβ fibril to NP-BSA$_x$-Sia-coated wells, increasing concentrations of free sialic acid were added to the wells, which reduced the amount of Aβ retained in the wells (Figure 5b). This suggests that free sialic acid can compete with NPs for Aβ binding, supporting the notion that interactions of Aβ with NP-BSA$_x$-Sia involve sialic acid.

2.6. NP-BSA$_x$-Sia Selectively Bound with Aβ Peptide Immobilized on Mouse Brains, which can be Detected via MRI

To test the feasibility and selectivity of Aβ detection by NPBSA$_x$-Sia, an ex vivo model was established by soaking brains from wild type mice in a suspension of Aβ fibrils for 24 h. After washing off unbound Aβ, the Aβ-adsorbed brains were then incubated with NP-BSA$_x$-Sia at 37 °C for 12 h. After removing unbound NPs, T_2* weighted MRI was performed on the brains. As shown in Figure 6a, significant darkening was observed on the surface of Aβ brains incubated with NP-BSA$_x$-Sia. The darkening in MR images was attributed to loss of MR signals due to NP binding. The presence of NP on the brain was confirmed by Prussian blue staining, which reacted with ferric ions to give intense blue color on the brain (Figure 6e). The binding of NP-BSA$_x$-Sia to Aβ soaked brain was sialic acid dependent, as addition of free sialic acid during NP incubation greatly reduced the sizes of areas with signal losses in MR images of the brains (Figure 6b) as well as the intensities of Prussian blue staining (Figure 6f).

In contrast to Aβ soaked brains, incubation of NP-BSA$_x$-Sia with mouse brains not coated with Aβ did not lead to much darkening of T_2* weighted MR images of the brains (Figure 6c) or significant blue color after Prussian blue staining (Figure 6g). In addition, Aβ soaked mouse brains did not yield any changes in T_2* weighted MR images by themselves (Figure 6d), nor did they give significant Prussian blue staining (Figure 6h). These results

collectively suggest that NP-BSA$_x$-Sia bound Aβ immobilized on a brain with high selectivity, with little or no binding of NPs by brain tissues in the absence of Aβ.

2.7. NP-BSA$_x$-Sia Enabled In Vivo Imaging of Aβ Plaques in a Human AD Mouse Model

To test the possibility of Aβ detection in vivo, a human AD model utilizing double transgenic (Tg) mice was established. These mice express a chimeric mouse/human amyloid precursor protein (Mo/HuAPP695swe) and a mutant human presenilin 1 (PS1-dE9) at central nervous system neurons. Both mutations are associated with early onset AD. These mice secrete human Aβ peptides, which are known to form Aβ plaques as those in humans. [60,61]

Tg mice in the age range of 39–42 weeks were used for in vivo Aβ plaque detection studies. When these mice were imaged directly by T_2* weighted MRI using a 3D gradient echo sequence, no abnormalities could be observed, suggesting that plaques were invisible under this condition (Figure 7b,d). Following administration of NP-BSA$_x$-Sia, contrast changes in brains were continuously monitored by MRI. Distinct dark spots due to loss of signals were observed in multiple slices of the brain in both cortex and hippocampus regions 1 h after injection of NP-BSA$_x$-Sia (Figures S4 and S5d, Supporting Information). The relative contrast changes reached their maximum values between 1 and 3 h. The signal changes lasted more than 1 d with the intensities returning to preinjection levels after 72 h (Figure 7a). Multiple slices and locations showed significant signal decreases upon NP-BSA$_x$-Sia administration (Figure 7c,e and Figures S4 and S5d (Supporting Information)). The signal changes were not due to presence of NPs in the blood as the signal intensities from the brain blood vessels returned to basal levels 2 h after NP administration (Figure 7a and Figure S6 (Supporting Information)).

For control experiments, NP-BSA$_x$-Sia was injected to age matched wild type mice, which do not express human Aβ in the brain. In contrast to Tg mice, no hypointense spots were observed in T_2* weighted images of the brains of wild type mice (Figure S5a,b, Supporting Information). To further verify the importance of NP-BSA$_x$-Sia in Aβ imaging, Feridex, a type of commercially available superparamagnetic iron oxide NPs, were injected to Tg mice at the same dose of Fe (8 mg kg^{-1}) as NP-BSA$_x$-Sia. No dark spots were observed in the brain in T_2* weighted images of these brains, suggesting that little Feridex particles were retained in the brains of Tg mice (Figure S7, Supporting Information).

2.8. Histological Analysis Confirmed the Presence of NP in Brains of Tg Mice after Administration of NP-BSA$_x$-Sia

Four hours after injection of NP-BSA$_x$-Sia to Tg mice, their brains were harvested and subjected to histological analysis. Thioflavin-s staining on AD brain slices showed punctate patterns of staining, confirming the presence of Aβ plaques in these brains (Figure 8a,b) in contrast to wild type mice (Figure 8c). Prussian blue staining showed the blue coloration on slices in hippocampus and cortex (Figure 8d,e), supporting the penetration and retention of NP-BSA$_x$-Sia into the brain. In brains of wild type mice after NP administration, Prussian blue failed to show any blue staining (Figure 8f,g), consistent with MR images observed in vivo, indicating the absence of NPs in these brains.

3. Discussion

While the etiology of AD has not been firmly established, AD detection based on biomarker such as Aβ can potentially provide early intervention of the disease to improve patient prognosis. Samples from the cerebrospinal fluid (CSF) obtained through lumbar puncture can allow the analysis of fluids surrounding the brain, reflecting key aspects of pathology.[62] The invasive nature of this approach renders it not ideal for routine evaluation of AD. Compared to CSF, blood samples are more readily available. However, extensive research aimed at identifying blood-based biomarkers has not led to satisfactory results.[63–65] With the possibility of directly imaging Aβ, MRI-based neuroimaging methods aided by NP contrast agents provide an attractive alternative for early detection of AD.

One significant hurdle in delivering NPs to the central nervous system is the BBB, due to the tight junctions between brain endothelial cells lining brain vascular vessels. NPs including magnetic NPs have been shown to bind Aβ in vitro.[43,66,67] However, presumably due to their poor abilities to penetrate into brains, they are not useful for in vivo brain imaging. These results are consistent with our observations using the iron oxide magnetic NP Feridex, as no significant contrast changes have been observed in T_2* weighted images of AD mouse brains after administration of Feridex and clearance of the particles from blood circulation (Figure S7, Supporting Information). It is well known that PEGylation can passivate NPs and improve their tissue penetration.[68] Polyethylene glycol (PEG) molecules have been installed on Aβ(1-42) peptide bearing iron oxide NPs, which enhanced their abilities to cross the BBB. One drawback is that retention of these NPs has also been observed in brains of normal mice in T_2* weighted MR images, which can possibly produce false positive identification.[14]

Receptor mediated transcytosis is another strategy to facilitate BBB penetration, which immobilizes ligands on NPs to target endocytic receptors expressed on brain endothelial cells.[69] The efficiency of transport across the BBB using this approach is restricted by the number of receptors exposed on brain endothelial cell surface. In addition, the ligand for binding the endocytic receptor may compete against that for Aβ binding for the limited number of conjugation sites on NP surface, lowering targeting efficiency.

Rather than relying on hypotonic mannitol to temporarily open up BBB, PEGylation of NPs, or receptor mediated transcytosis, we explored cationized BSA coating (Figure 1) to facilitate NP entries into the brain. The brain endothelial cells are polarized with the luminal side presenting high net negative charges. As a result, positively charged compounds such as cationized BSA can cross BBB from blood vessels through an absorptive transcytosis process by binding with clathrin-coated pits or caveolae for transport across the cells.[70] Applying this idea to NP transport,[71–73] the interactions of sialic acid coated cationized magnetic NPs with brain endothelial cells bEnd.3 were investigated using a variety of techniques. These NPs could readily bind and be taken up by bEnd.3 cells, as confirmed by flow cytometry and confocal microscopy (Figure 3). Furthermore, the internalized NPs could be released from the cells (Figure 4a). The combined endocytosis and exocytosis processes should enable high cellular penetration of NP-BSA$_x$-Sia. To demonstrate this, multiple layers of bEnd.3 cells were grown on a transwell filter, which mimics BBB due to

the restricted free diffusion of molecules across the cells indicated by the high TEER values. NP-BSA$_x$-Sia was found to readily transcytose through the multilayer brain endothelial cells (Figure 4b), suggesting its potential to enter brains without the need for exogenous agents such as mannitol to open up BBB.

Biocompatibility is another important parameter for in vivo applications as some biological probes can cause significant toxicities. For example, cationic nanoparticles can not only disrupt cell membranes due to their interactions with negatively charged cell surface but also cause lysosomal and mitochondrial damages.[74] Glycosylation can be an effective approach to reduce the toxicities of probes.[75] In our study, the NP-BSA$_x$ showed significant toxicities to bEnd.3 cells at doses above 0.25 mg NP mL^{-1} (Figure 2). For in vivo mouse imaging studies, 8 mg Fe kg^{-1} NP administered was equivalent to a blood concentration of 0.8 mg NP mL^{-1}, suggesting that the NP-BSA$_x$ was undesirable due to toxicity concerns. This difficulty is overcome by sialic acid functionalization of the NPs, which greatly improved biocompatibility of the NPs (Figure 2), while maintaining the abilities to transport across BBB.

Sialic acid is an underexplored ligand for Aβ binding studies. Sialic acid interacts with Aβ through binding with *N*-terminal amino acids especially His13.[34] While the binding of a single sialic acid molecule with Aβ is relatively weak, incorporation of multiple copies of sialic acid onto a NP can significantly enhance the avidity through the multivalent effect. The NP-BSA$_x$-Sia on average contains 118 copies of sialic acid per particles, which is similar to our previous design of NP-Sia for Aβ binding.[43] More than 100-fold higher concentrations of free sialic acid were needed to disrupt the binding of Aβ with NP-BSA$_x$-Sia in competitive ELISA assay (Figure 5b), confirming the enhanced avidity of sialic acid presented on the NPs. The introduction of sialic acid onto NP-BSA$_x$ not only reduced the inherent toxicity of the NPs, but also facilitated NP binding with Aβ. NP-BSA$_x$-Sia exhibited excellent selectivities toward Aβ binding as demonstrated by the ex vivo staining of Aβ coated brains (Figure 6e–h).

Upon administration of NP-BSA$_x$-Sia to AD mice, the region of interest-based quantitative measurement of T_2* values from the in vivo MRI showed significant reduction of T_2* values in both cortex and hippocampus areas of the brain, attributed to NP binding to Aβ plaques (Figure 7). The contrast changes lasted more than 1 d, which were not due to the presence of NPs in the blood as the contrast of the blood vessel lumen returned to preinjection levels in about 2 h (Figure 7a). Histology studies also supported the retention of NPs in AD mouse brains (Figure 8). In contrast to aforementioned PEGylated NPs, little NPs were found in normal mouse brains after administering with NP-BSA$_x$-Sia (Figure S5, Supporting Information). Presumably in these mice, due to the absence of Aβ plaques, the NP-BSA$_x$-Sia was not retained in brain tissues after BBB penetration.

4. Conclusion

Sialic acid coated BSA magnetic NPs were synthesized, which bound to Aβ deposit in brains with high selectivity. The NP-BSA$_x$-Sia could penetrate the BBB and enable detection of Aβ plaques using MRI in an AD mouse model without the need for mannitol to

open up the BBB. This overcomes a significant hurdle in NP aided Aβ plaque imaging. Sialic acid functionalization of the NPs greatly improved the biocompatibility of the probe with enhanced Aβ binding avidity. With further development, such probes can aid in longitudinal monitoring of Aβ plaque development as well as the evaluation of potential novel therapeutic interventions to reduce Aβ plaque loads.

5. Experimental Section

Animal

39–42 weeks old B6C3-Tg (APPswe/PS1dE9) mice and age matched wild type C57BL/6 mice were used for this study. Animals were purchased from Jackson Laboratories and were kept in the University Laboratory Animal Resources Facility of the Michigan State University. All the experimental procedures for animal study were performed with approval of the Institutional Animal Care and Use Committee of the Michigan State University.

Assessment of NP-BSA$_x$-Sia Binding with Aβ Fibril via ELISA

The binding of NP-BSA$_x$-Sia to Aβ fibril was determined by an ELISA. In order to prepare Aβ fibril, synthetic Aβ(1-42) (1 mg) was dissolved in 1,1,1,3,3,3 hexafluoro-2-propanol (3 mL) and after sonication, it was lyophilized to remove the solvent. The resulting thin peptide film was dissolved in an aqueous solution of 10×10^{-3} M NaOH (0.25 mL). After 10 min of sonication, the peptides were neutralized with diluted HCl solution to pH = 6, and diluted in PBS buffer (pH = 7.2) to the desired final concentrations. The Aβ fibrils were obtained after incubation of the monomers at 37 °C for 48 h without stirring. The obtained fibrils along with NP-BSA$_x$-Sia were used for ELISA studies. For each well of a 96 well plate (Nunc MaxiSorp flat-bottom), a NP-BSA$_x$-Sia solution (0.5 mg mL^{-1}, 50 μL) was added. After overnight incubation at 37 °C, the NPs adhered to the bottom of the wells. Then, the wells were washed with PBST (3×, 300 μL each) and different concentrations of Aβ solutions (50 μL of 0.09×10^{-6}, 0.37×10^{-6}, 1.48×10^{-6}, 6.0×10^{-6}, 23.75×10^{-6}, and 95.0×10^{-6} M, respectively) were added to the NP-BSA*x*-Sia coated wells, respectively, and incubated at 22 °C for 12 h followed by thorough washing with phosphate buffered saline solution with Tween® (PBST) (3×). Anti-Aβ(1-16) Immunoglobulin G (IgG) (6E10) monoclonal antibody (50 μL per well, 0.137×10^{-9} M, 1:24 000 in 1% (w/v) BSA containing PBS) was added and after 1 h incubation at 22 °C, wells were washed with PBST (3×) and the solution was discarded. The amount of Aβ bound was quantified by the absorbance change of each well upon incubation with the goat anti-mouse HRP conjugated secondary antibody (50 μL, 1.7×10^{-9} M, 1:18 000 in 1% (w/v) BSA in PBS). The solution was discarded and the wells were washed with PBST (3×). A mixture of H_2O_2 (20 μL) and freshly prepared 3,3′,5,5′-tetramethylbenzidine (TMB) solution (5 mg TMB dissolved in dimethyl sulfoxide (DMSO) (2 mL) and then diluted with citrate phosphate buffer to 20 mL) was prepared and this mixture (150 μL) was added to the ELISA wells. The blue color was allowed to develop for 10–20 min, then the reaction was quenched by adding an aqueous solution of H_2SO_4 (0.5 M, 50 μL) and the absorbance was measured at 450 nm on an iMark microplate reader. To further establish the role of sialic acid in Aβ binding, a competitive ELISA was performed when a fixed amount of Aβ (0.5×10^{-6} M, 50 μL) was added to NP-BSA$_x$-Sia coated plates

together with increasing concentrations of free sialic acid (50 μL each; 0.00013, 0.00052, 0.0021, 0.0084, 0.033, and 0.135 M, respectively).

Assessment of NP-BSA$_x$-Sia Transcytosis through bEnd.3 Endothelial Cells

bEnd.3 cells were cultured in a 100 mm cell culture plate at 37 °C and 5% CO_2 till it reached 80% confluency. Cells were trypsinized, collected by centrifugation, and resuspended in 10% fetal bovine albumin–Dulbecco's modified Eagle medium (DMEM) to a final concentration of 1.3×10^5 cells mL^{-1}. Serum containing DMEM (1.5 mL) was added to the wells of a 12-well plate, above which the transwell inserts were placed. The cell suspension (500 μL) was added to each transwell (6.72×10^4 cells per transwell). The plate was incubated at 37 °C and 5% CO_2 for two weeks. The growth medium was changed every day. The integrity of the multilayered cell culture was assessed by TEER measurements using a Millicell-ERS Volt-Ohm Meter (Millipore). Transendothelial electrical resistance after the period of two weeks was found to be 133 Ω cm^2. After two weeks, the growth medium was removed and the cell layer was washed with PBS. Serum free DMEM (1.5 mL) was added to the bottom of the 12-well plate wells. Two transwells received NP-BSA$_x$-Sia-FITC in serum-free DMEM (0.5 mL, 0.32 mg mL^{-1}). Aliquots (100 μL) were drawn at different time points from the lower compartment and the fluorescence was assessed on a plate reader (excitation wavelength 488 nm; emission wavelength 520 nm). After measurement, the aliquots were returned to their respective wells. The volume in the bottom wells was maintained at 1.5 mL.

In Vivo Imaging

NP-BSA$_x$-Sia was dispersed in PBS (100 μL) and administered to mice via retro-orbital injection at a dose of 0.14 mmol Fe kg^{-1} body weight. Isoflurane (2.5% in oxygen) was used for anesthesia induction for about 5 min and isoflurane (1–1.5% in oxygen) was used to maintain the anesthesia. A circulatory water bath was used to keep the mouse body temperature consistent around 35 °C. The breathing rate was monitored during scans and it was controlled around 20 min^{-1} to minimize motion artifacts. MRI scans were performed on a Bruker 7 T BioSpec 70/30 USR MRI. Images were acquired with a dedicated mouse brain coil (four channel array) at 100 μm isotropic resolution using a 3D_FLASH sequence, flip angle = 15°, echo time = 8 ms, time of repetition = 30 ms, receiver bandwidth = ±16 kHz, field of view = 19.2 × 19.2 × 16 mm, number of averages = 2, and number of excitation = 2.

40 week old female Tg mice were scanned before injection and at different time intervals (0.5, 1, 1.5, 2, 24, and 72 h) post injections. Images collected were analyzed using NIH ImageJ software. The signal intensities of spots undergoing changes following NP injection were measured and they were normalized by dividing the measured intensity by the average intensity of brain tissues with no dark spots and these normalized values were plotted against time. As a control for Tg mice model of AD, NP-BSA$_x$-Sia was injected at the same iron concentration to wild type mice and images were collected and analyzed as described above. To further examine the ability of NP-BSA$_x$-Sia for binding to amyloid plaques, commercially available dextran coated iron oxide NP (Feridex) was injected to Tg mice and the images were analyzed in a similar manner.

Supplementary Material

Refer to Web version on PubMed Central for supplementary material.

Acknowledgments

S.H.N. and H.K. contributed equally to this work. The authors are grateful for the financial support from the National Institute of General Medical Sciences, the NIH (R01GM072667), and the Michigan State University toward this project. The authors would like to thank the Department of Radiology, Michigan State University, for generously providing MRI scanner time.

References

1. Prince, M., Comas-Herrera, A., Knapp, M., Guerchet, M., Karagiannidou, M. World Alzheimer Report 2016: Improving Healthcare for People Living with Dementia: Coverage, Quality and Costs Now and in the Future. Alzheimer's Disease International (ADI); London, UK: 2016.
2. [accessed: October 2017] Alzheimer's Disease Facts and Figures. 2016. https://www.alz.org/documents_custom/2016-facts-and-figures.pdf
3. Mueller SG, Weiner MW, Thal LJ, Petersen RC, Jack CR, Jagust W, Trojanowski JQ, Toga AW, Beckett L. Alzheimer's Dementia. 2005; 1:55.
4. Graham WV, Bonito-Oliva A, Sakmar TP. Annu Rev Med. 2017; 68:413. [PubMed: 28099083]
5. Hardy J, Selkoe DJ. Science. 2002; 297:353. [PubMed: 12130773]
6. Chetelat G, Villemagne VL, Bourgeat P, Pike KE, Jones G, Ames D, Ellis KA, Szoeke C, Martins RN, O'Keefe GJ, Salvado O, Masters CL, Rowe CC. Ann Neurol. 2010; 67:317. [PubMed: 20373343]
7. Johnson KA, Minoshima S, Bohnen NI, Donohoe KJ, Foster NL, Herscovitch P, Karlawish JH, Rowe CC, Carrillo MC, Hartley DM, Hedrick S, Pappas V, Thies WH. Alzheimer's Dementia. 2013; 9:E1.
8. Klunk WE, Engler H, Nordberg A, Wang YM, Blomqvist G, Holt DP, Bergstrom M, Savitcheva I, Huang GF, Estrada S, Ausen B, Debnath ML, Barletta J, Price JC, Sandell J, Lopresti BJ, Wall A, Koivisto P, Antoni G, Mathis CA, Langstrom B. Ann Neurol. 2004; 55:306. [PubMed: 14991808]
9. Klunk WE, Lopresti BJ, Ikonomovic MD, Lefterov IM, Koldamova RP, Abrahamson EE, Debnath ML, Holt DP, Huang GF, Shao L, DeKosky ST, Price JC, Mathis CA. J Neurosci. 2005; 25:10598. [PubMed: 16291932]
10. Vanhoutte G, Dewachter I, Borghgraef P, Van Leuven F, van der Linden A. Magn Reson Med. 2005; 53:607. [PubMed: 15723413]
11. Jack CR, Wengenack TM, Reyes DA, Garwood M, Curran GL, Borowski BJ, Lin J, Preboske GM, Holasek SS, Adriany G, Poduslo JF. J Neurosci. 2005; 25:10041. [PubMed: 16251453]
12. Braakman N, Matysik J, van Duinen SG, Verbeek F, Schliebs R, de Groot HJM, Alia A. J Magn Reson Imaging. 2006; 24:530. [PubMed: 16892201]
13. Jack CR, Garwood M, Wengenack TM, Borowski B, Curran GL, Lin J, Adriany G, Gröhn OH, Grimm R, Poduslo JF. Magn Reson Med. 2004; 52:1263. [PubMed: 15562496]
14. Wadghiri YZ, Li J, Wang J, Hoang DM, Sun Y, Xu H, Tsui W, Li Y, Boutajangout A, Wang A, de Leon M, Wisniewski T. PLoS One. 2013; 8:e57097. and references cited therein. [PubMed: 23468919]
15. Tanifum EA, Ghaghada K, Vollert C, Head E, Eriksen JL, Annapragada A. J Alzheimer's Dis. 2016; 52:731. [PubMed: 27031484]
16. Viola KL, Sbarboro J, Sureka R, De M, Bicca MA, Wang J, Vasavada S, Satpathy S, Wu S, Joshi H, Velasco PT, MacRenaris K, Waters EA, Lu C, Phan J, Lacor P, Prasad P, Dravid VP, Klein WL. Nat Nanotechnol. 2015; 10:91. [PubMed: 25531084]
17. Wadghiri, YZ., Hoang, DM., Wisniewski, T., Sigurdsson, EM. Amyloid Proteins: Methods and Protocols. 2. Sigurdsson, EM.Calero, M., Gasset, M., editors. Vol. 849. Springer; New York, USA: 2012. p. 435-451.

18. Poduslo JF, Wengenack TM, Curran GL, Wisniewski T, Sigurdsson EM, Macura SI, Borowski BJ, Jack CR. Neurobiol Dis. 2002; 11:315. [PubMed: 12505424]
19. Petiet A, Santin M, Bertrand A, Wiggins CJ, Petit F, Houitte D, Hantraye P, Benavides J, Debeir T, Rooney T, Dhenain M. Neurobiol Aging. 2012; 33:1533. [PubMed: 21531045]
20. Pardridge WM. NeuroRx. 2005; 2:3. [PubMed: 15717053]
21. Brightman MW. Exp Eye Res. 1977; 25:1.
22. Aparicio-Blanco J, Martin-Sabroso C, Torres-Suárez AI. Biomaterials. 2016; 103:229. [PubMed: 27392291]
23. Rapoport SI. Cell Mol Neurobiol. 2000; 20:217. [PubMed: 10696511]
24. Yang J, Wadghiri YZ, Hoang DM, Tsui W, Sun Y, Chung E, Li Y, Wang A, de Leon M, Wisniewski T. NeuroImage. 2011; 55:1600. [PubMed: 21255656]
25. Wadghiri YZ, Sigurdsson EM, Sadowski M, Elliott JI, Li Y, Scholtzova H, Tang CY, Aguinaldo G, Pappolla M, Duff K, Wisniewski T, Turnbull DH. Magn Reson Med. 2003; 50:293. [PubMed: 12876705]
26. Sillerud LO, Solberg NO, Chamberlain R, Orlando RA, Heidrich JE, Brown DC, Brady CI, Vander Jagt TA, Garwood M, Vander Jagt DL. J Alzheimer's Dis. 2013; 34:349. [PubMed: 23229079]
27. Salloway S, Sperling R, Fox NC, Blennow K, Klunk W, Raskind M, Sabbagh M, Honig LS, Porsteinsson AP, Ferris S, Reichert M, Ketter N, Nejadnik B, Guenzler V, Miloslavsky M, Wang D, Lu Y, Lull J, Tudor IC, Liu E, Grundman M, Yuen E, Black R, Brashear HR. N Engl J Med. 2014; 370:322. [PubMed: 24450891]
28. Ostrowitzki S, Deptula D, Thurfjell L, Barkhof F, Bohrmann B, Brooks DJ, Klunk WE, Ashford E, Yoo K, Xu ZX, Loetscher H, Santarelli L. Arch Neurol. 2012; 69:198. [PubMed: 21987394]
29. Sperling R, Salloway S, Brooks DJ, Tampieri D, Barakos J, Fox NC, Raskind M, Sabbagh M, Honig LS, Porsteinsson AP, Lieberburg I, Arrighi HM, Morris KA, Lu Y, Liu E, Gregg KM, Brashear HR, Kinney GG, Black R, Grundman M. Lancet Neurol. 2012; 11:241. [PubMed: 22305802]
30. Cheng KK, Chan PS, Fan S, Kwan SM, Yeung KL, Wang YX, Chow AH, Wu EX, Baum L. Biomaterials. 2015; 44:155. [PubMed: 25617135]
31. Hu B, Dai F, Fan Z, Ma G, Tang Q, Zhang X. Adv Mater. 2015; 27:5499. [PubMed: 26270904]
32. Kouyoumdjian, H., Huang, X. Carbohydrate Nanotechnology. Stine, KJ., editor. John Wiley & Sons, Inc; Hoboken, New Jersey, USA: 2016. p. 309-333.
33. Wang B. Annu Rev Nutr. 2009; 29:177. [PubMed: 19575597]
34. Williamson MP, Suzuki Y, Bourne NT, Asakura T. Biochem J. 2006; 397:483. [PubMed: 16626304]
35. Zha Q, Ruan Y, Hartmann T, Beyreuther K, Zhang D. Mol Psychiatry. 2004; 9:946. [PubMed: 15052275]
36. Matsuzaki K, Horikiri C. Biochemistry. 1999; 38:4137. [PubMed: 10194329]
37. Ariga T, Kobayashi K, Hasegawa A, Kiso M, Ishida H, Miyatake T. Arch Biochem Biophys. 2001; 388:225. [PubMed: 11368158]
38. Ariga T, Yu RK. Neurochem Res. 1999; 24:219. [PubMed: 9972868]
39. Patel DA, Henry JE, Good TA. Brain Res. 2007; 1161:95. [PubMed: 17604005]
40. Patel D, Henry J, Good T. Biochim Biophys Acta. 2006; 1760:1802. [PubMed: 16982154]
41. Chikae M, Fukuda T, Kerman K, Idegami K, Miura Y, Tamiya E. Bioelectrochemistry. 2008; 74:118. [PubMed: 18676183]
42. Dhavale D, Henry JE. Biochim Biophys Acta. 2012; 1820:1475. [PubMed: 22565051]
43. Kouyoumdjian H, Zhu DC, El-Dakdouki MH, Lorenz K, Chen J, Li W, Huang X. ACS Chem Neurosci. 2013; 4:575. [PubMed: 23590250]
44. Krol S. J Controlled Release. 2012; 164:145.
45. Xie J, Peng S, Brower N, Pourmand N, Wang SX, Sun S. Pure Appl Chem. 2006; 78:1003.
46. Yim YS, Choi JS, Kim GT, Kim CH, Shin TH, Kim DG, Cheon J. Chem Commun. 2012; 48:61.
47. Smith KR, Borchardt RT. Pharm Res. 1989; 6:466. [PubMed: 2762222]
48. Warren L. J Biol Chem. 1959; 234:1971. [PubMed: 13672998]

49. Li G, Simon MJ, Cancel LM, Shi ZD, Ji X, Tarbell JM, Morrison B III, Fu BM. Ann Biomed Eng. 2010; 38:2499. [PubMed: 20361260]
50. Brown RC, Morris AP, O'Neil RG. Brain Res. 2007; 1130:17. [PubMed: 17169347]
51. Omidi Y, Campbell L, Barar J, Connell D, Akhtar S, Gumbleton M. Brain Res. 2003; 990:95. [PubMed: 14568334]
52. Butterfield DA, Swomley AM, Sultana R. Antioxid Redox Signaling. 2013; 19:823.
53. Bravo R, Arimon M, Valle-Delgado JJ, García R, Durany N, Castel S, Cruz M, Ventura S, Fernàndez-Busquets X. J Biol Chem. 2008; 283:32471. [PubMed: 18819917]
54. Teplow, DB. Methods in Enzymology. Wetzel, R., Kheterpal, I., editors. Vol. 413. Academic Press; San Diego, USA: 2006. p. 20-33.
55. Bitan G, Vollers SS, Teplow DB. J Biol Chem. 2003; 278:34882. [PubMed: 12840029]
56. Bitan G, Teplow DB. Methods Mol Biol. 2005; 299:3. [PubMed: 15980591]
57. Lesné S, Koh MT, Kotilinek L, Kayed R, Glabe CG, Yang A, Gallagher M, Ashe KH. Nature. 2006; 440:352. [PubMed: 16541076]
58. Shankar GM, Li S, Mehta TH, Garcia-Munoz A, Shepardson NE, Smith I, Brett FM, Farrell MA, Rowan MJ, Lemere CA, Regan CM, Walsh DM, Sabatini BL, Selkoe DJ. Nat Med. 2008; 14:837. [PubMed: 18568035]
59. Klein WL, Krafft GA, Finch CE. Trends Neurosci. 2001; 24:219. [PubMed: 11250006]
60. Reiserer RS, Harrison FE, Syverud DC, McDonald MP. Genes, Brain Behav. 2007; 6:54. and references cited therein. [PubMed: 17233641]
61. Chin J. Methods Mol Biol. 2011; 670:169. [PubMed: 20967591]
62. Blennow K, Zetterberg H. Front Neurosci. 2015; 9:345. [PubMed: 26483625]
63. Irizarry MC. NeuroRx. 2004; 1:226. [PubMed: 15717023]
64. O'Bryant SE, Gupta V, Henriksen K, Edwards M, Jeromin A, Lista S, Bazenet C, Soares H, Lovestone S, Hampel H, Montine T, Blennow K, Foroud T, Carrillo M, Graff-Radford N, Laske C, Breteler M, Shaw L, Trojanowski JQ, Schupf N, Rissman RA, Fagan AM, Oberoi P, Umek R, Weiner MW, Grammas P, Posner H, Martins R. Alzheimer's Dementia. 2015; 11:549.
65. Blennow K, Hampel H, Weiner M, Zetterberg H. Nat Rev Neurol. 2010; 6:131. [PubMed: 20157306]
66. Zhou J, Fa H, Yin W, Zhang J, Hou C, Huo D, Zhang D, Zhang H. Mater Sci Eng, C. 2014; 37:348.
67. Yang CC, Yang SY, Chieh JJ, Horng HE, Hong CY, Yang HC, Chen KH, Shih BY, Chen TF, Chiu MJ. ACS Chem Neurosci. 2011; 2:500. [PubMed: 22860173]
68. Nance EA, Woodworth GF, Sailor KA, Shih TY, Xu Q, Swaminathan G, Xiang D, Eberhart C, Hanes J. Sci Transl Med. 2012; 4:149ra119.
69. Jones AR, Shusta EV. Pharm Res. 2007; 24:1759. [PubMed: 17619996]
70. Hervé F, Ghinea N, Scherrmann JM. AAPS J. 2008; 10:455. [PubMed: 18726697]
71. Saraiva C, Praça C, Ferreira R, Santos T, Ferreira L, Bernardino L. J Controlled Release. 2016; 235:34.
72. Chuang VT, Kragh-Hansen U, Otagiri M. Pharm Res. 2002; 19:569. [PubMed: 12069157]
73. Lu W, Zhang Y, Tan YZ, Hu KL, Jiang XG, Fu SK. J Controlled Release. 2005; 107:428.
74. Fröhlich E. Int J Nanomed. 2012; 7:5577.
75. He XP, Zang Y, James TD, Li J, Chen GR, Xie J. Chem Commun. 2017; 53:82.

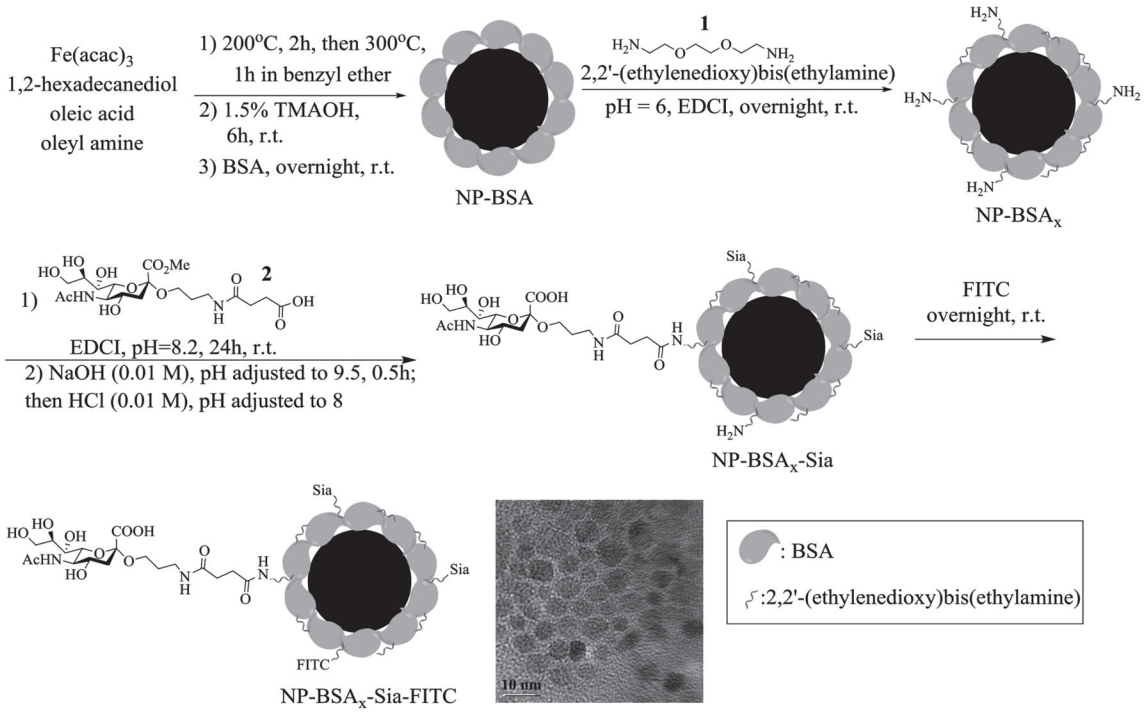

Figure 1.

Synthesis of NP-BSA$_x$-Sia and NP-BSA$_x$-Sia-FITC. The scale bar for TEM image is 10 nm.

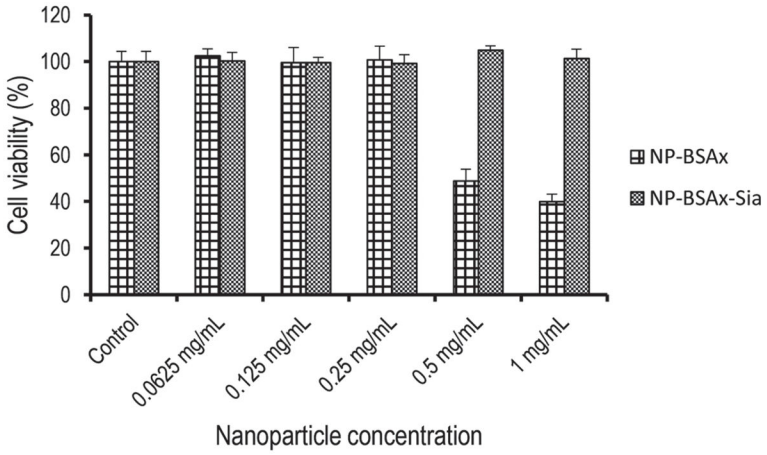

Figure 2.

Viability of bEnd.3 cells following treatment with various concentrations of NP-BSA$_x$ and NP-BSA$_x$-Sia. While NP-BSA$_x$ exhibited cytotoxicity above 0.25 mg mL^{-1}, NP-BSA$_x$-Sia did not cause any toxicities in the concentrations examined.

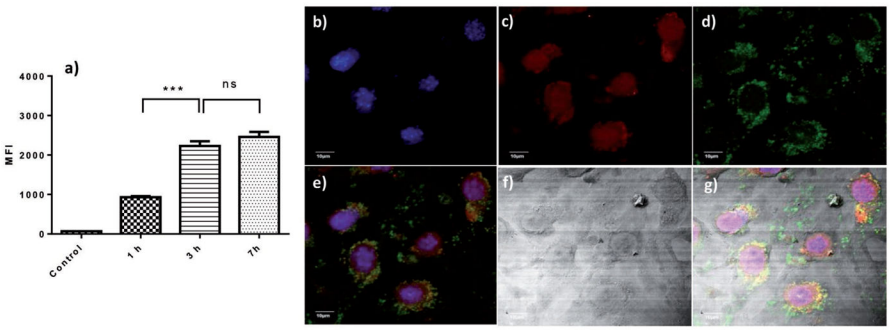

Figure 3.

NP-BSA$_X$-Sia-FITC binding and uptake by bEnd.3 cells: a) Time dependent increase of bEnd.3 cells upon incubation with NP-BSA$_X$-Sia-FITC as measured by flow cytometry; b–g) confocal microscopy images of bEnd.3 cells after incubation with NPs, (b) DAPI channel showing locations of nuclei; (c) Lysotracker channel showing locations of lysosomes; (d) FITC channel showing locations of NPs; (e) overlay of (b–d), (f) DIC image of the cells; and (g) overlay of (e) and (f). The scale bar is 10 μm.

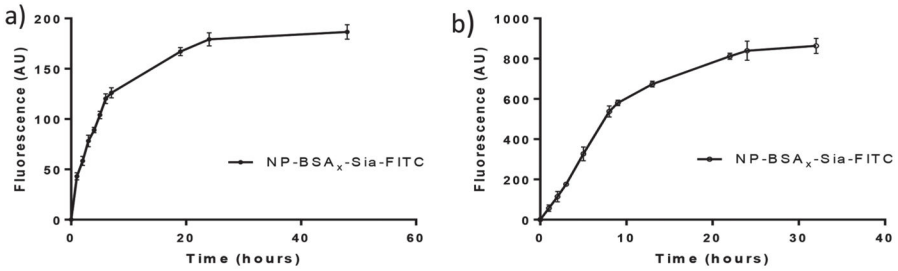

Figure 4.

a) Time dependent release of NP-BSA$_x$-Sia-FITC from bEnd.3 cells showed that internalized NPs can be exocytosed; b) NP-BSA$_x$-Sia-FITC can penetrate through multilayers of bEnd.3 cells in a transwell assay.

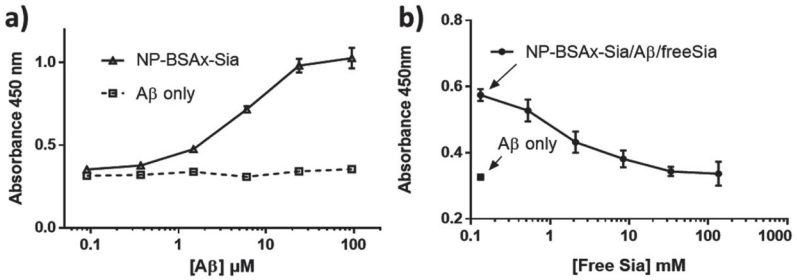

Figure 5.

a) ELISA showed dose dependent binding Aβ by immobilized NP-BSA$_x$-Sia with an apparent binding constant of 3 μm. b) Free sialic acid can reduce Aβ binding to immobilized NP-BSA$_x$-Sia in a dose dependent manner, suggesting that the binding of Aβ with NP-BSA$_x$-Sia is dependent on sialic acid. Wells containing Aβ (0.5×10^{-6} M) binding to NP-BSA$_x$-Sia with varying concentrations of free sialic acid (circle) and Aβ (0.5×10^{-6} M) binding to bare wells (square).

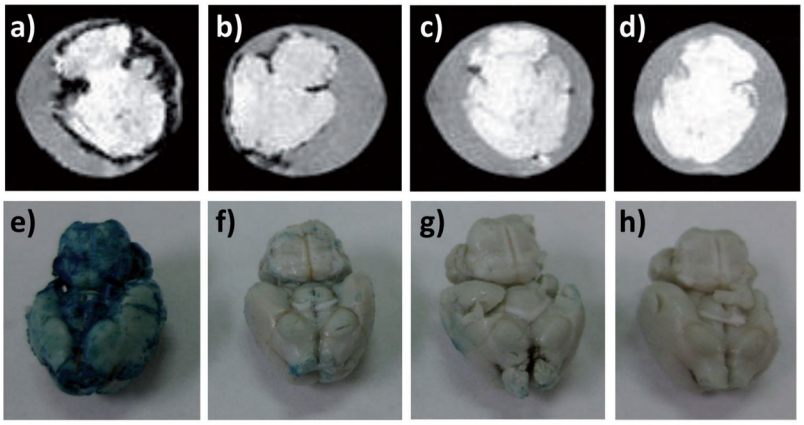

Figure 6.

T_2* weighted MR and Prussian blue staining images of an ex vivo model of AD brains. T_2* weighted MR images of a) Aβ mouse brain incubated with NP-BSA$_X$-Sia; b) Aβ mouse brain incubated with NP-BSA$_X$-Sia in the presence of free sialic acid; c) normal mouse brain incubated with NP-BSA$_X$-Sia; and d) Aβ mouse brain. Prussian blue staining of e) Aβ mouse brain incubated with NP-BSA$_X$-Sia; f) Aβ mouse brain incubated with NP-BSA$_X$- Sia in the presence of free sialic acid; g) normal mouse brain incubated with NP-BSA$_X$-Sia; and h) Aβ mouse brain.

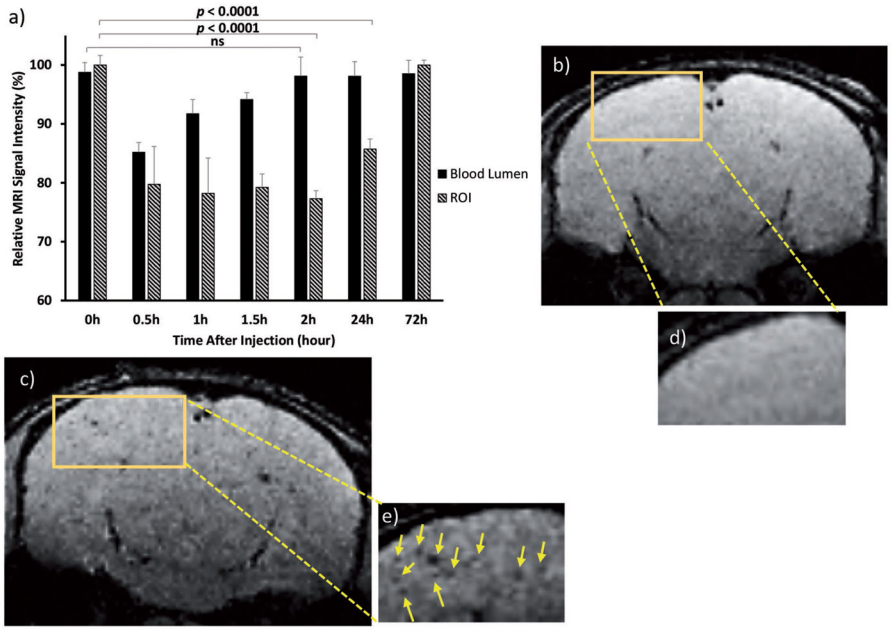

Figure 7.

T_2* weighted MRI signal intensity changes of Tg mouse brain before and after administration of NP-BSA$_X$-Sia. Mice were scanned at different time intervals (0.5, 1, 1.5, 2, 24, and 72 h) after NP administration. a) Quantification of relative signal intensity changes in one region of interest (ROI) versus blood vessel in the brain. The observed signal changes in the region of interests were presumably due to NP binding with Aβ plaques, not from the blood pool effect as contrast of brain blood vessels returned to basal levels 1 h after NP administration. The contrast changes in region of interest lasted more than 24 h. Statistical analysis was performed using Student's *t* test. Selected MR images showing contrast changes. MR images of mouse brain b) before NP injection; and c) 1.5 h after NP injection. d) Expansion of the boxed region of (b). e) Expansion of the boxed region of (c). The arrows indicate the location of contrast change.

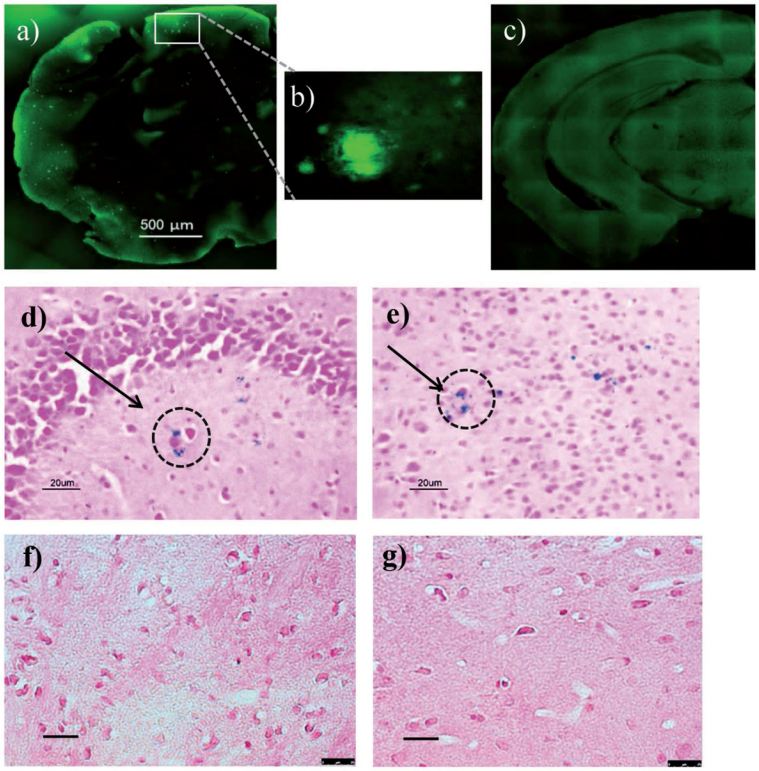

Figure 8.

a,b) Thioflavin-S staining of Tg mouse brain indicated the presence of Aβ deposition. The scale bar is 500 μm. c) Thioflavin-S staining of wild type mouse brain showed no Aβ plaques. d,e) Prussian blue staining of brain tissue from Tg mice following intravenous NP administration. Representative areas of Prussian blue staining are highlighted in the circles. The presence of blue staining confirms the presence of Fe in Tg mouse brain presumably due to NP accumulation. (d) showed the location of Fe near hippocampus and (e) in the cortex. f,g) Wild type mouse brain after intravenous NP administration showed no Prussian blue staining due to the absence of NPs in the brains. Scale bars are 20 μm.